International Journal for Housing Science and Its Applications
Publish August 10, 2025. Volume 46, Issue 4 Pages 2568-2584

https://doi.org/10.70517/ijhsa464216

Visualization management technology based on a three-dimensional control platform in power grid operation safety analysis

Yiming Tang[1,*], Yu Song[1] and Xingwei Zhang[1]
[1] Jiangsu Frontier Electric Technology Co., Ltd., Nanjing, Jiangsu, 211102, China
Corresponding authors: (e-mail: ymtang2025@126.com).

Abstract Electricity is an indispensable component of social development and people's daily lives, making its safe production and operation of utmost importance. In recent years, China has increasingly emphasized the importance of safe operation management, aiming to enhance safety risk control across all sectors. This paper establishes and improves the safety operation management system for power grids within a three-dimensional control platform, strengthening the management of power grid operations. From a probabilistic risk perspective, the safety level of power grid operation management measures is analyzed, enabling quantitative analysis of the consequences of power grid safety incidents. A safety risk assessment index for power grids is proposed, and transient safety risks are calculated. Using a Markov-type simulation of basic component models and state sampling methods, the system's safety risk assessment is conducted. Through simulation experiments, the voltage stability indicators of each load node under operational conditions are calculated. When the voltage enters an unstable warning state, the stability factors of nodes 4, 13, and 6 are relatively high, at 0.27485, 0.31856, and 0.38482, respectively. In terms of the precision of power operation safety visualization control, the highest control precision achieved by the method proposed in this paper reached 96.85%, improving the orderliness of power data and enabling the visualization control of the power information system to achieve relatively ideal results.

Index Terms three-dimensional control platform, probabilistic risk, Markov model, state sampling method, power grid safety

I. Introduction

In recent years, China has increasingly emphasized the importance of occupational safety and health management, aiming to enhance safety risk control across all sectors. As an indispensable component of social development and people's daily lives, the safety of the power sector is of critical importance [1]. However, power safety accidents or incidents still occur from time to time due to factors such as external operational environments, equipment operational conditions, unsafe behaviors of personnel, and inadequate management organization, causing severe negative impacts on social production development and the lives and property of the people [2]-[4]. Therefore, power companies must strengthen their risk management and control capabilities to improve their safety management levels [5].

With the rapid development of smart grids and information technology, China has transitioned from traditional grids to modern grids, entering a new phase marked by smart grids [6]. In this new development phase, on one hand, traditional risk management methods relying primarily on expert experience can no longer meet current safety management needs [7], [8]. On the other hand, there are significant deficiencies in the display of power grid operation risk management, such as limited information, insufficiently intuitive display effects, and a lack of human-machine interaction [9], [10]. Against the backdrop of digital transformation, technological and information-based methods have enabled the application and sharing of engineering data during the power grid operation phase, allowing for the dynamic display and accurate analysis of operational risks [11]-[13]. Meanwhile, the design of power grid management platforms is gradually transitioning from two-dimensional to three-dimensional digitalization [14]. Conventional two-dimensional design has certain limitations. Three-dimensional digital design enables precise design, facilitating three-dimensional spatial safety distance verification and material statistics [15], [16]. By establishing a unified collaborative design platform and adopting a centralized, real-time interactive work method, communication efficiency between interfaces can be improved, ensuring design accuracy [17]-[19]. Additionally, establishing three-dimensional model data enables integrated unit design based on attribute parameters, allowing real-time loading of unit design results in a three-dimensional

environment, thereby improving work efficiency [20]-[22]. Therefore, designing a visualization management platform based on three-dimensional control technology effectively enhances the visualization level of power grid operation risk warning and control, providing decision-making basis for power grid operation risk management.

The foundation for achieving intelligent risk management in power safety management is high-quality data from multiple sources. To this end, scholars have conducted research on safety risk management technologies for power grid systems. Literature [23] explores big data-driven energy management technologies, utilizing big data wind analysis techniques to mine the vast amounts of information data accumulated in the energy sector, providing decision-making basis for the management and operation of smart grids. Literature [24] proposes a new multi-objective energy management method for microgrids, which can analyze and optimize power fluctuations and peak shaving in grid interconnection lines, promote load balancing across the grid, and achieve safe and controllable grid operation. Literature [25] explores safety risk management measures for smart grids, which, through appropriate calculation and management, can significantly reduce safety threats posed by electronic communication services and provide scientific recommendations for the safe operation of smart grids. However, the information data involved in automated risk control is relatively formalized, which increases the cognitive threshold for operators and is not conducive to manual intervention.

The power grid operation risk control visualization system screens, processes, and analyzes the above-mentioned abstract massive data information and displays it in an intuitive and vivid manner to reveal the status, patterns, or trends of the system. Reference [26] established a grid visualization prediction system based on grid functionality and geographic knowledge, which can visualize real-time and historical information data, assisting operators in observation and analysis. Reference [27] indicates that grid operation status visualization analysis can combine the advantages of human experience and data analysis methods, playing a significant role in addressing related grid issues. Literature [28] designed a power system visualization tool integrating multiple technologies such as artificial neural networks. By monitoring the operational status of the power grid and visually displaying relevant analytical data, it achieves effective control of power grid operational risks. Literature [29] noted that traditional power system data analysis suffers from the issue of abundant data but scarce information. Therefore, a visualization analysis model based on power big data was constructed, which not only enhances the accuracy of power data analysis but also lowers the operational threshold for business personnel. Literature [30] developed a joint electromechanical visualization simulation platform for floating wind turbines, which can perform visualization analysis of mechanical and electrical information data under the same wind and wave conditions, providing data support for related tasks in offshore wind power generation. Therefore, the visualization analysis system achieves human-machine interaction in power system safety risk monitoring, ensuring more stable operation of the power system. Based on this, further integration of three-dimensional models, real-world scenarios, and power grid operational status information, combined with different types and attributes of information for multi-dimensional dynamic visualization and analysis, can present the overall operational status of the power grid in a more intuitive manner.

This paper focuses on improving and standardizing the management systems for “work permits,” “operation permits,” shift handover procedures, and anti-misoperation devices based on power grid operational safety. Considering the actual operational conditions of the power grid, this paper strengthens management over transformer equipment, operational modes, and relay protection systems. By analyzing the risk status of the power system, this paper conducts a quantitative analysis of the potential consequences of events that may pose risks, thereby obtaining the assessment results for power grid operational safety. Establish grid safety risk instability probability assessment indicators, use multi-dimensional K-means clustering technology, and construct a multi-level load model. Considering the two states of component operation and failure, establish a Markov-type component model to conduct transient safety risk assessments. Utilize simulation experiments to assess grid operational safety. Apply scene segmentation algorithms to model three-dimensional visualization scenes, design a three-dimensional control platform, and validate visualization control technologies through testing experiments.

II. Grid safety operation management measures based on a three-dimensional control platform

II. A. Establish and implement safety management systems

Establishing and continuously improving on-site safety management systems for substations is an important means and fundamental prerequisite for ensuring the long-term safe and stable operation of the power grid. Under normal circumstances, substations should focus on improving and standardizing the following management system requirements.

II. A. 1) Work Permit Management System

All work activities at the substation site must be carried out in accordance with the “work permit.” No on-site work or operations may be conducted without a valid “work permit.” After reviewing and approving the contents of the “work permit,” the safety measures outlined therein must be implemented, and on-site operations and requirements must be verified. Once all criteria are met, the appropriate markings must be made.

II. A. 2) Work Permit Management System

Specifically, an “operation ticket” is a standardized procedure established for different operations, requiring strict adherence to the specified procedures during on-site operations. After inspection and approval, the ticket is signed off. Taking switchgear operation as an example, the operation steps must be predefined and the “operation ticket” filled out correctly. After ticket review and successful rehearsal, the operation objectives and hazard points are clarified, and hazard point pre-control measures are implemented. The operation instructions and timing issued by the dispatcher are accepted. A comprehensive inspection of equipment names, numbers, and status is conducted. Operations are conducted in accordance with the content of the “work permit,” repeatedly implementing the process of “reading the permit—repeating—supervising—operating.” After completing the operation as required, mark it accordingly. Report the completion of the operation and time information to the dispatch department, record the operation, and after verification, sign off on the “work permit.”

II. A. 3) Shift handover management system

It is required that the handover records be filled out correctly and comprehensively to ensure that all personnel are fully informed of the substation's operational status, equipment conditions, and on-site work status.

II. A. 4) Misoperation Prevention Device Management System

When developing a misoperation prevention device management system, it is necessary to focus on three key areas: misoperation prevention device anomaly management, misoperation prevention interlock device operation and maintenance, and emergency unlock key management.

II. B.Increase focus on and management of power grid operations

II. B. 1) Strengthening the management of substation equipment

There are relatively many factors associated with the operation of substation equipment, so it is necessary to increase investment in substation equipment management to effectively maintain the safety level of power grid operation. Among these factors, line aging plays a significant role in affecting the operation of substation equipment. This requires relevant personnel to regularly conduct inspections of the current status of substation equipment circuits, promptly replace circuits with severe aging issues, and implement maintenance and upkeep for circuits that can continue to be used. Real-time monitoring of the operational process of substation equipment is necessary to promptly address any abnormalities and ensure the safe and stable operation of substation equipment, thereby ensuring that its performance and functionality are effectively utilized.

II. B. 2) Strengthening management of operating modes

Analyze the actual operating conditions of the power grid and propose as many scientifically sound and reasonable operating schemes as possible, setting equipment parameters to ensure that the corresponding operating schemes can maximize their advantages [31]. In practice, it is necessary to conduct an in-depth and comprehensive analysis of the grid's operational mode to ensure that the grid can maintain a safe and stable operational state, while the entire operational process is economically viable and reasonable. Based on this, the management of operational modes must be standardized to ensure that defects can be promptly identified and addressed with targeted measures. Additionally, efforts should be intensified in operational safety prevention work, with contingency plans developed for different types of incidents and regular emergency drills conducted to provide a robust foundation for the long-term safe and stable operation of the grid.

II. B. 3) Strengthening relay protection work

Conduct rigorous inspections and maintenance of the structural components of pressure plates, control and protection equipment, fuses, and other devices to ensure that the relay protection system can swiftly transition to operational status following a power grid operational incident. Under both power-off and power-on conditions, analyze the operational status of the relay protection system. When accident equipment suddenly trips, also analyze the operational status of the relay protection system to ensure its stable operation. During this process, focus on inspecting the operational status of indicator lights, the integrity of fuses and contacts, and other aspects to ensure that the relay protection system effectively fulfills its role in maintaining grid safety and stable operation.

III. Assessment of grid operation safety included in system management methods

III. A. Application of Safety Risk Assessment in Power Grid Operation

The International Council on Large Electric Systems (CIGRE) first introduced the concept of power system risk assessment in 1997 [32]. Power system safety risk assessment requires analyzing the risk state of the power system and conducting quantitative analysis of the consequences of events that may pose risks. Calculating the probability of failure events occurring and the severity of their consequences are both essential. In actual power grid planning, since the focus is on the consequences of specific faults, the deterministic “N-1” criterion (single-element fault criterion) is typically used to measure the reliability level of the system. Deterministic assessment methods conduct qualitative analyses of system safety through accident verification, primarily evaluating the likelihood of system instability and the amount of load shedding. This method has several issues: first, it ignores the randomness of components and does not consider the probability of system operating modes. Second, it can only anticipate the consequences of certain low-severity fault types and determine whether the system remains stable under such fault conditions. Third, it fails to reflect users' requirements for system safety and reliability levels at the evaluation and decision-making stage of planning schemes, thereby affecting the accuracy of safety and reliability indicator assessments. In contrast, probabilistic risk assessment is based on the probabilistic failure modes of components, taking into account uncertainties across all aspects of the system, and can accurately quantify the probabilistic impact of failure events. It can be said that risk assessment methods provide an important approach for quantifying safety indicators in power grid planning. Therefore, in planning schemes that require consideration of power grid safety, the safety level of the planning scheme should be analyzed from the perspective of probabilistic risk. That is, it is not only necessary to consider the consequences of failure accidents but also to account for the probability of their occurrence, converting safety levels into quantifiable risk indicators to provide a unified scale for measuring system safety and economic efficiency.

III. B. Grid Safety Assessment Indicators

Large-scale power grid safety risk assessment indicators can be divided into two major categories: system indicators and fault event indicators. The former reflects the overall safety level of the system, while the latter indicates the impact of individual fault events on system safety. System indicators can be further categorized into system instability probability, frequency, and expected load shedding, among others. Fault event indicators include fault event instability probability, instability duration, instability frequency, and expected load shedding, among others. Since the primary focus of large-scale power grid safety risk assessment is on the system's safety and stability, the assessment process places greater emphasis on system indicators. Additionally, the algorithm in this paper ranks the severity of accidents and the importance of components based on risk indicators to facilitate comparison with deterministic criteria.

Common large-scale power grid safety risk evaluation indicators include the following:

(1) Probability of instability (PLOS) [33]:

$$PLOS = \sum_{i \in SW \text{ Set of unstable states}} \begin{matrix} \text{Probability } P_i \text{ of the} \\ \text{system handling unstable state } i \end{matrix} \tag{1}$$

(2) Probability of loss of stability (PLOPAS):

$$PLOPAS = \sum_{\substack{i \in SW \text{ Set of power angle} \\ \text{instability states}}} \begin{matrix} \text{Probability } P_i \text{ of state } i \text{ causing} \\ \text{power angle instability in the system} \end{matrix} \tag{2}$$

(3) Probability of voltage instability PLOVS:

$$PLOVS = \sum_{\substack{i \in SW \text{ Set of voltage} \\ \text{instability states}}} \begin{matrix} \text{State } i \text{ causing system} \\ \text{voltage instability Probability } P_i \end{matrix} \tag{3}$$

(4) Probability of frequency instability PLOFS:

$$PLOFS = \sum_{\substack{i \in SW \text{ Set of frequency} \\ \text{instability states}}} \begin{matrix} \text{State } i \text{ causing system frequency} \\ \text{instability Probability } P_i \end{matrix} \tag{4}$$

(5) The general definition of transient risk indicators is as shown in Equation (5):

$$R = \sum_{i=1}^{N_C} P(n)S(n) \tag{5}$$

In the equation, R is the system transient risk index, N_C is the number of system fault states, $P(n)$ is the probability of system state n, and n is the severity function of system state n. Since system transient stability is actually power angle stability, the severity function $S(n)$ is defined as in equation (6):

$$S = \frac{1}{M_{total}T}\int_0^T \sum_{i=1}^{NG} M_i \left[\max(\delta_i^t - \delta_{COI}^t - \delta^{\max}, 0, \delta_{COI}^t - \delta_i^t - \delta^{\max})\right]^2 dt \tag{6}$$

In the equation, NG is the number of generators, T is the duration of the transient process of the generator's power angle swing, M_i is the rotational inertia of generator i, and M_{total} is the sum of the rotational inertias of all generators. δ_i^t is the power angle of generator i at time t, and δ_{COI}^t is the power angle of the center of inertia COI at time t, which also serves as the reference value for the power angles of all generators. δ_{COI}^t is defined as follows:

$$\delta_{COI}^t = \frac{\sum_{i=1}^{NG} M_i \delta_i^t}{M_{total}} \tag{7}$$

Therefore, if the power angle of the generator relative to the center of inertia COI is δ, then $S(n)$ can measure the degree of deviation of δ relative to $\pm\delta_{\max}$ during the transient process T of power angle oscillation. If the value of $S(n)$ is 0, it indicates that the system is transiently stable under the fault condition. If the value of $S(n)$ is not 0, it indicates that the system is unstable under the fault condition, and the larger the value of $S(n)$, the more severe the system instability.

III. C. Principles of power grid security assessment considering system management methods

When conducting safety assessments of actual power systems, analyses typically only consider the maximum load operating mode, resulting in risk indicators that often deviate from actual outcomes. If these risk indicators are incorporated into grid planning decisions, they can significantly impact the accuracy of optimal planning solutions. Therefore, to improve the accuracy and precision of risk assessment, this paper considers the system's operating mode and its probability in transient safety risk assessment. The safety risk assessment incorporating the system's operating mode primarily includes three main aspects: (1) establishing typical system operating modes, (2) determining component state models and selecting system states and their probabilities, and (3) assessing the consequences of the selected system states and calculating transient safety risk indicators.

III. C. 1) Typical System Operating Modes

In risk assessment methods, clustering techniques are typically used to establish a multi-level load model that can incorporate the correlations of all load curves. Based on multidimensional K mean clustering techniques, the steps for obtaining typical system operating modes include [34]:

(1) Obtain the annual load duration curve of the system and divide it into X curves according to the percentage of peak load

(2) Randomly generate initial values for i cluster means M_{ij}. Here, $j(j=1,\cdots,X)$ denotes the j th curve.

(3) Calculate the Euclidean distance from each load point at every time step to each cluster mean:

$$D_{ki} = \left[\sum_{j=1}^{X}\left[(M_{ij} - L_{kj})^2\right]\right]^{1/2} \tag{8}$$

Among them, L_{kj} represents the k th load value in the j th curve.

(4) Based on the calculated Euler distance values, assign each load point at each time to the cluster with the smallest Euler distance. Then reclassify all load points and recalculate the cluster mean M_{ij}:

$$M_{ij} = \sum_{k=1}^{N_i} L_{kj} / N_i \tag{9}$$

In this context, N_i denotes the total number of load points in the i th cluster.

(5) Repeat steps (3) and (4) until all cluster means remain unchanged during the iteration process.

In the multi-level load model, the converged cluster mean M_{ij} represents the load level of the i th cluster under the j th curve. At the same time, the corresponding proportion of generator output is used as the multi-level power generation output level.

III. C. 2) System Component Failure Model

Markov models are often used to simulate basic component models, and are particularly common when using state sampling methods for system safety risk assessment. Markov models can describe components such as

transmission lines, transformers, busbars, generators, and so on. When only considering the two states of component operation and failure, a two-state model of the component can be obtained, as shown in Figure 1.

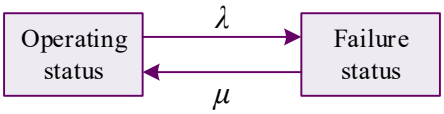

Figure 1: Two-state model

In the equation, λ and μ represent the failure rate and repair rate of the component, respectively. When the failure density function of the component follows an exponential distribution, the failure rate and repair rate of the component are both constants. These two parameters are related to the mean time to failure $MTTF$ and the mean time to repair $MTTR$ as follows. Generally, when two of the parameters are known, the other two can be calculated:

$$\lambda = 1 / MTTF \tag{10}$$

$$\mu = 1 / MTTR \tag{11}$$

According to Equations (10) and (11), the failure probability U of the component can be obtained as:

$$U = \frac{\lambda}{\lambda + \mu} \tag{12}$$

For any component i in the power system, a uniform distribution in the interval $[0,1]$ can be used for simulation. Let X_i denote the operating state of component i, which is expressed by equation (13):

$$X_i = \begin{cases} 0, & \text{If } R_i \geq U_i, \text{Component failure} \\ 1, & \text{If } 0 < R_i < U_i, \text{Component branch} \end{cases} \tag{13}$$

In the formula, R_i represents a uniformly distributed random number in the interval $[0,1]$ generated by component i, and U_i represents the failure probability of component i.

When conducting transient safety risk assessment, the Monte Carlo method is used to randomly sample all possible component failure states to obtain the system state vector X with N components:

$$X = \left(X_1, X_2, \ldots, X_k, \ldots, X_N\right) \tag{14}$$

After a component failure occurs, determining the system status is relatively complex, involving multiple aspects such as the failed component, failure location, failure type, protection and switch operation status, etc. The Markov equation can be used to calculate indicators such as system status probability, frequency, and duration.

III. C. 3) Security assessment steps for system management methods

After selecting one or more fault events using the Monte Carlo sampling method to determine the system state, transient stability digital simulation is required to determine whether the system state is stable, typically using time-domain methods. Additionally, disturbance sequences must be specified in transient stability simulation calculations. Different faults result in different disturbance sequences. These sequences include not only switching operations and reclosing but also various safety and stability measures such as generator tripping and load shedding.

This paper is based on the state-space method and uses PSD-BPA power flow and transient stability software for relevant analysis and calculations. Combining the steps for obtaining the operating mode, the steps for the safety risk assessment method considering the system operating mode are as follows:

(1) Based on the annual load duration curve and generator output, cluster N typical system operating modes.

(2) Generate N system power flow and stability data files corresponding to the operating modes.

(3) Read in the data file for one system operating mode.

(4) Randomly sample faulty lines, select fault locations and types.

(5) Determine the system's operational state and its probability.

(6) Conduct transient stability simulation under the system's current state to determine if the system can maintain stability. If it can, return to step (4); if not, implement certain safety corrective measures, including reactive power equipment engagement, generator tripping, load shedding, system decoupling, etc., and analyze post-accident risks.

(7) Determine whether the maximum simulation count has been reached. If not, return to step (4); if so, calculate the transient safety risk index for the system state.

(8) Determine whether the system operating mode calculation is complete. If not, return to step (2); if so, output the final results. The safety risk assessment flowchart for the system operating mode is shown in Figure 2.

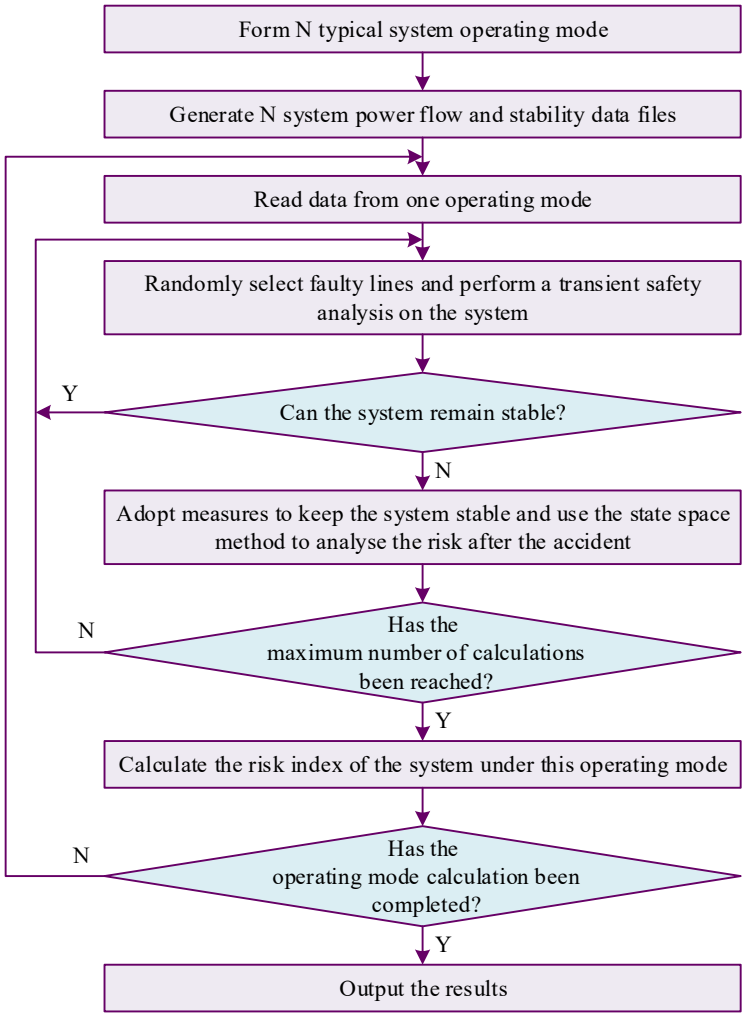

Figure 2: Consider the security risk assessment of the system operation mode

III. D. Case Study Analysis

III. D. 1) Simulation Event 1

By gradually increasing the active and reactive power of PQ nodes and PV nodes in the whole network with the constant power factor, the voltage and current phasors of each node at different load rates can be obtained as synchronous measurement data of the power grid operation system.

In the calculation, the threshold value of d_i is 0.02, and the minimum stability margin η is 0.1.

When the system is operating normally, only the admittance sensitivity factor d_i of each load node needs to be monitored. When the load increases to η=1.8581, d_{10}=0.01858 is detected, the voltage instability warning is detected, and the stability factor k_i of each load node is calculated. When the load increases to η=2.24866, the stability factor k_8=0.92748 of node 6 exceeds the limit and enters the voltage instability emergency state. Table 1 shows the voltage stability index of each load node of the system under different operating conditions. When the voltage enters the instability warning state, k_4, k_{13}, k_6 are higher, which are 0.27485, 0.31856 and 0.38482, respectively.

Fig. 3 and Fig. 4 are the instability factor k_i with load and V-A curve of nodes 6, 13 and 4, respectively, and the horizontal axis λ is the growth factor of load and generator output. Combined with Table 1, it can be seen that in the emergency state of voltage instability, the stability factors of nodes 6, 13 and 4 are the largest, which are 0.92748, 0.88486 and 0.80785, respectively, and the corresponding voltages are 0.21955, 0.64852 and 0.36425,

respectively, and it can be seen from Figure 4 that although the voltage of node 13 is higher at this time, it is very close to its critical voltage, so it is easy to cause voltage collapse. According to the value of the stability factor k of each load node, nodes 6, 13 and 4 can be identified as weak nodes of system voltage, and are used as key nodes for load control in the next step.

Table 1: The voltage stability indicator of each load node in different running state

Node	Normal state		Voltage instability warning status			Voltage instability emergency state		
	Voltage	d	Voltage	d	k	Voltage	D(10^{-3})	K
2	1.03485	0.07856	0.92585	0.04585	0.14858	0.79852	0.22485	0.41648
4	1.00485	0.11648	0.85485	0.06996	**0.27485**	0.66958	**0.36425**	**0.80785**
5	0.99642	0.05985	0.85696	0.02485	0.17852	0.64348	0.13485	0.41634
6	0.99648	0.06487	0.84528	0.04855	**0.38482**	0.64855	**0.21955**	**0.92748**
8	1.00644	0.11648	0.84988	0.06558	0.08985	0.65424	0.31964	0.17458
9	1.01858	0.11348	0.87425	0.06369	0.16485	0.71869	0.30348	0.53482
10	1.03699	0.05987	0.91652	**0.01858**	0.10855	0.78642	0.08485	0.44855
11	0.99484	0.05365	0.91464	0.02996	0.07452	0.78469	0.15748	0.22468
13	1.03486	0.70856	0.94348	0.26489	**0.31856**	0.90185	**0.64852**	**0.88486**
15	1.04685	0.15489	0.91785	0.07855	0.14856	0.79855	0.28486	0.43485
17	1.03985	0.24965	0.97596	0.09458	0.10542	0.90485	0.25948	0.34895
18	1.04985	0.09878	0.92485	0.04856	0.13887	0.80485	0.19848	0.44188
20	1.03485	0.10998	1.00348	0.04758	0.10448	0.94788	0.22486	0.23485
21	1.05485	0.06636	0.94282	0.03969	0.06482	0.85269	0.16768	0.20748
22	1.03485	0.11854	0.91648	0.06324	0.15748	0.79254	0.36486	0.45588
23	1.05489	0.23489	0.96485	0.09848	0.10685	0.88493	0.43418	0.42485
24	1.04856	0.35485	0.98189	0.11489	0.08585	0.92485	0.40846	0.54855
Total load	49.8485+j11.5448		95.0486j22.0485			111.748e+j25.864		

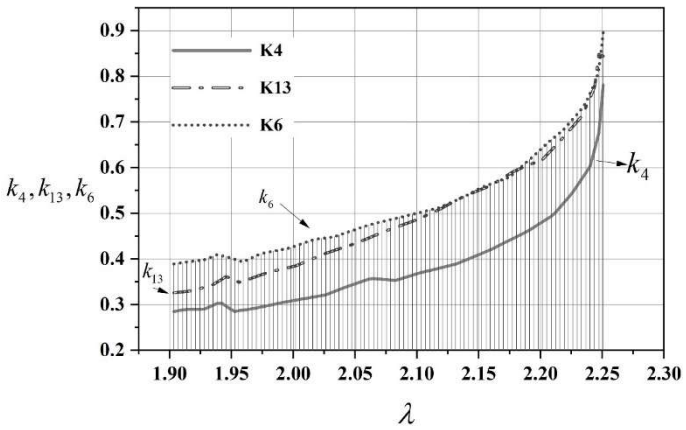

Figure 3: k_4, k_{13}, k_6 With the load change curve

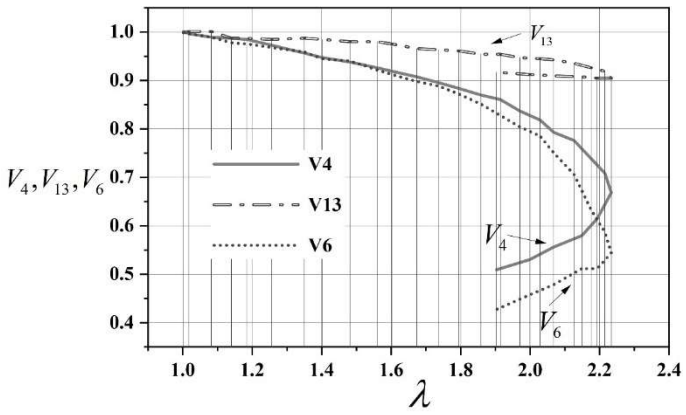

Figure 4: Load node's $V-\lambda$ characteristic curve

III. D. 2) Simulation Event 2

Gradually increase the active and reactive loads of node 6 with a constant power factor, while keeping the loads of other nodes unchanged. The increased load is borne by the balancing node.

The calculation process takes into account reactive power overlimit. When the PV node exceeds the reactive power limit, it is converted to a PQ node for calculation. The specific situation in the calculation is as follows: when the load factor λ=1.7685, PV node 34 exceeds the reactive power limit, When λ = 1.8696, PV node 32 exceeds the reactive power limit; when λ = 1.8755, PV node 35 exceeds the reactive power limit; when λ = 1.9631, PV node 33 exceeds the reactive power limit.

Table 2 shows the stability factor values k_i for each node when the system is nearing instability. When the system is approaching the voltage collapse point with a load factor λ=1.96311, the stability factor values k_i for each node are as follows. Among them, node 6 has the largest k value, k_6 = 0.9815, so node 6 can be identified as the weakest node.

Table 2: The stability factor k_i value of each node in the near instability

Node	k_i	Node	k_i
2	0.0849	15	0.0748
4	0.1785	17	0.0763
5	0.1169	18	0.0796
6	**0.9815**	20	0.0415
8	0.0349	21	0.0342
9	0.0946	22	0.0761
10	0.0812	23	0.0981
11	0.0396	24	0.1342
13	0.2485		

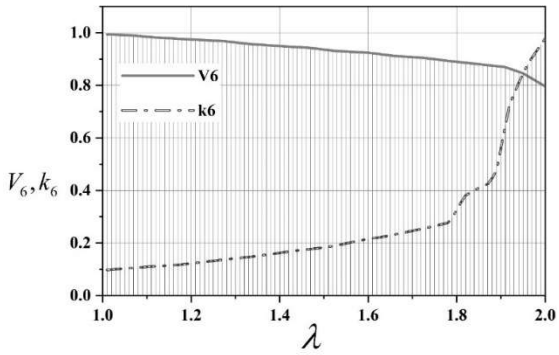

Figure 5: The voltage and stability factor of node 6 varies with load

Figure 5 shows the voltage and stability factor curves of Node 6 as a function of load variation. The several inflection points on the curve correspond to multiple instances of reactive power exceeding limits at PV nodes. When λ = 1.8696, the reactive power limit violation at PV node 32, which is close to node 6, changes to PQ node, causing a significant increase in the slope of the k_6 curve. This is because node 6 loses a large amount of reactive power support, leading to rapid voltage instability at this node when the load further increases.

As can be seen from the above simulation analysis, the stability factor k_i curve shows good monotonicity overall and can effectively identify weak nodes in the system's voltage. On the other hand, the stability factor k_i can correctly reflect dynamic changes in the system, such as reactive power exceeding limits, and the calculation results are more consistent with the actual situation of the system.

III. D. 3) Grid Security Assessment

Based on the power grid safety evaluation index model proposed in this paper, five regions of the same scale were selected from the State Grid for safety evaluation. The values of each index were calculated using the original data, and the extreme value method was used to normalize the calculation of each index. Specifically, for positive indices, the maximum value was taken as 1. For negative indices, the minimum value was taken as 1. Finally, all indices were dimensionless, with values ranging from 0 to 1. The coefficient of variation method was used to calculate the weights of each indicator for the five regions. Specifically, the standard deviation and coefficient of variation were calculated for each indicator, and all indicators were normalized to obtain their respective weights. Finally, the comprehensive linear scoring method was used to conduct a comprehensive evaluation of power grid operational safety, with the results shown in Table 3.

Based on the evaluation results, overall, Region 5 has the highest grid safety score of 0.65485, followed by Regions 4, 3, and 2, with Region 1 having the lowest safety score of 0.22795. Relatively speaking, Region 5 has higher positive indicator values, such as an N-1 test pass rate of 94.37486% and a unit line power supply of 1,338.248 million kW•h/km, while negative indicator values are relatively low, such as 72 substation accidents and 28 transmission accidents. The expected power shortage duration of 7.33487 hours is also the lowest. Some indicators, such as the transformer load rate of 43.61254 and the transformer capacity-to-load ratio of 3.964285, although their values are relatively low, have low weights and thus have a limited impact on the overall safety of the power grid. Region 1 has the lowest grid safety level at 0.22795, while Region 5's safety level is 0.4269 higher than Region 1's. This is not only because Region 1's overall indicators are lower, but also because the weights of indicators such as transformer load factor, voltage stability, and transmission accident frequency are high, while their values are low, which significantly affects the overall safety level of Region 1's grid. The evaluation results are consistent with the actual safety levels of the grids in each region.

Table 3: The comprehensive evaluation results of power grid safety

First-indicator	Secondary indicators	Third indicators	Region 1	Region 2	Region 3	Region 4	Region 5
Safety	Structural safety	N-1 Check qualification rate	85.64254	88.24899	90.05495	91.54928	**94.37486**
		Transformer load rate	43.49595	45.16485	43.84969	43.97485	43.61254
		Transformer capacity ratio	4.785779	3.954834	4.452494	3.845621	3.964285
		Unit line power supply	1061.595	1165.079	1234.648	1280.918	**1338.248**
	Safe operation	Number of electrical accidents	332	293	200	100	**72**
		Number of transmission accidents	136	108	65	48	**28**
	Stability	Frequency stability	99.94864	99.94862	99.94482	99.94687	99.81648
		Voltage stabilization	99.84968	99.84152	99.93158	99.96428	99.95424
		Rotation reserve rate	3.54968	2.49395	7.24895	4.84956	6.54678
	Abundance	Low power expected	32.54199	12.56974	18.54984	8.84965	7.33487
Comprehensive evaluation of power grid safety			0.22795	0.37486	0.60458	0.62796	0.65485
Ranking			5	4	3	2	1

IV. Visualization of power grid safety management based on a three-dimensional control platform

IV. A. Platform Overview

IV. A. 1) Upper-layer application system functional design

The upper-layer application system of the visualization system consists of three components: the large-screen visualization subsystem, virtual scene demonstration, and augmented reality interactive applications, as shown in Figure 6. The basic functions of each component are decomposed to form a detailed functional model of the upper-layer application system. The upper-level application system utilizes data processing technology to process the massive amounts of multi-source data from the power system through a series of processing steps, presenting it in a more intuitive and multi-dimensional manner on the large screen. It also employs digital sensing technology and human-machine interaction technology to enable virtual scene demonstrations and augmented reality interactive applications, providing a smarter and more efficient approach to daily safety management in the power system.

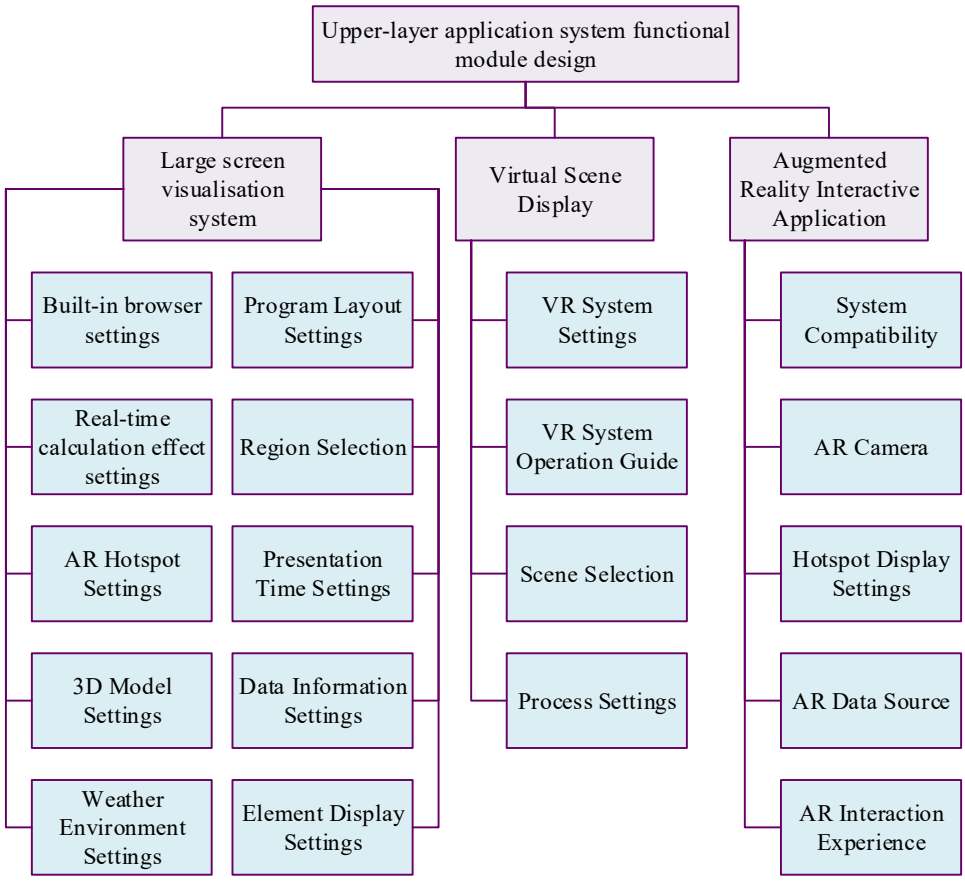

Figure 6: Design of functional modules for upper-level application systems

IV. A. 2) Design of underlying support platform functions

The underlying support platform for the visualization system consists of three components: a 3D model library, the Unity3D dynamic editing platform, and an SQL database, as shown in Figure 7. The basic functions of each component are broken down individually to form a detailed functional model of the underlying support platform. The underlying support platform utilizes 3D modeling and optimization techniques, real-time rendering technology, and database technology to achieve model creation, scene interaction, and data storage functions, providing data, models, and scenes to support the display functions of upper-level applications.

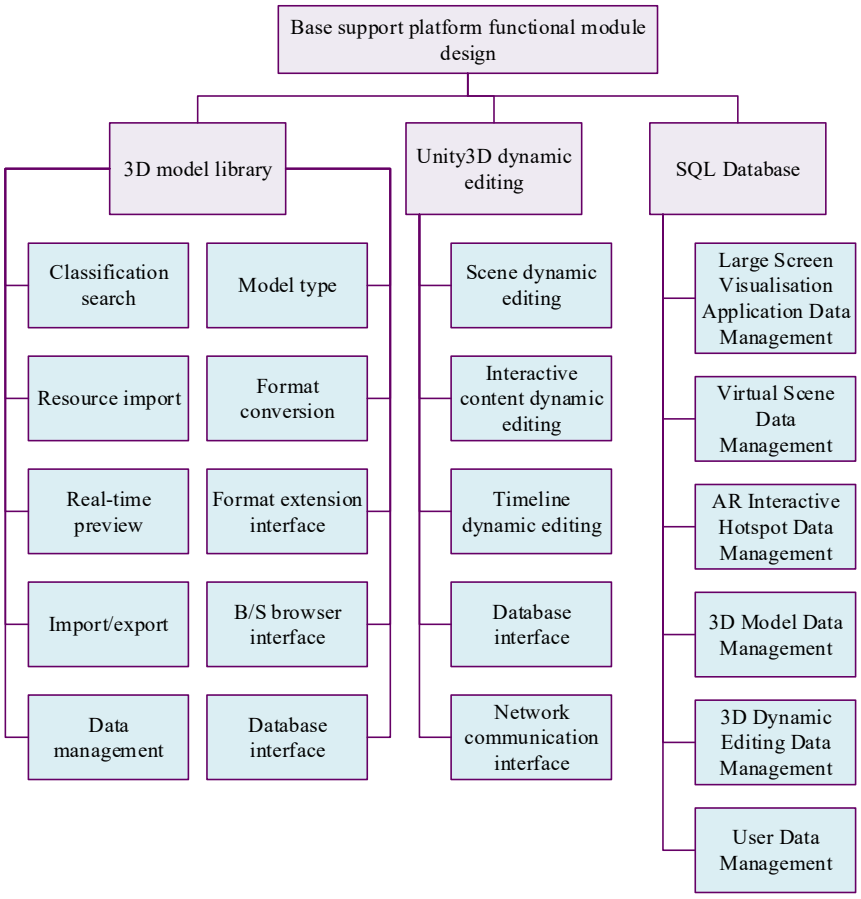

Figure 7: The design of the underlying support platform's functional modules

IV. B. Three-dimensional control platform design

IV. B. 1) Scene segmentation algorithm

In the process of visualizing the 3D control platform, the most critical step is scene management. The dispatch room handles a significant volume of business operations, resulting in a large number of scenes. When considering each piece of equipment and cabinet, the number of scenes can reach the ten-thousand level. Organizing static and dynamic objects within numerous scenes, describing the relationships between scenes and objects, and optimizing rendering time for 3D images are key challenges that scene management must address.

Figure 8 illustrates spatial scene segmentation. For the power 3D control platform, traditional scene management algorithms are difficult to apply directly due to the complexity of the scenes and the interactivity during maintenance processes. Therefore, this paper employs a scene management method based on cost functions. In this method, it is necessary to construct the cost function to be used and select spatial plane segmentation factors.

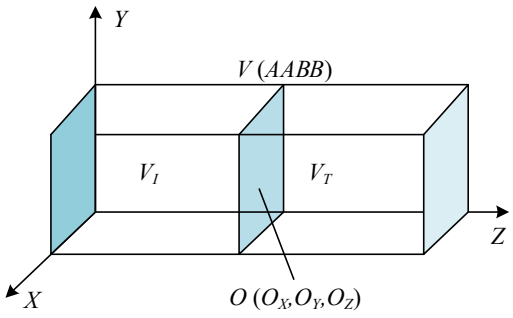

Figure 8: Spatial scene segmentation illustration

$V(AABB)$ indicates that the space is covered by an $AABB$ box scene. The lengths of the box in the X,Y,Z directions are l_x,l_y,l_z, respectively, and the coordinates of the center of the box $V(AABB)$ in the three-dimensional coordinate system are $O(O_x,O_y,O_z)$. Assume that a plane perpendicular to the *XOZ* plane is drawn through the center of the traversal box $V(AABB)$, dividing it into two parts, V_l and V_r, to the left and right, respectively. Let the distance from the origin of the coordinate system to the dividing plane be x, and the surface areas of V_l and V_r be $S(V_l)$ and $S(V_r)$, respectively. Suppose there are uniform and parallel light rays in the space, and let P_l and P_r be the probabilities of the light rays hitting the left and right spaces, respectively. Then:

$$P_l = \frac{S(V_l)}{S(V)} = \frac{l_x l_y + l_x l_z + l_y x}{l_x l_y + l_x l_z + l_y l_z} \tag{15}$$

$$P_r = \frac{S(V_r)}{S(V)} = \frac{l_x l_y + l_x (l_z - x) + l_y (l_z - x)}{l_x l_y + l_x l_z + l_y l_z} \tag{16}$$

In scene segmentation algorithms, the computational resources consumed during segmentation must be calculated, which is referred to as the traversal cost function $C(V)$. For a computer room, the traversal of the scene is C_t, and the cost generated when a triangle intersects a straight line in the scene is Ci. At this point, the cost of the entire space is:

$$C(V) = C_t + P_l \times C(V_l) + P_r \times C(V_r) \tag{17}$$

When performing scene segmentation, to achieve real-time dynamic control of objects, objects must be treated as the smallest management units. During spatial segmentation, the integrity of the bounding boxes surrounding objects must be maintained. Therefore, it is essential to select appropriate segmentation factors. Assuming that there are $V_1,V_2,\cdots,V_m$ bounding boxes coexisting in the space, the cost function for each subspace segmentation can be obtained. At the same time, the partial derivative of this cost function in the X direction is calculated:

$$C'_x = \left(\frac{2l_m + 2l_n}{l_m l_n + l_m l_p + l_n l_p} \times y - \frac{l_m n + l_n n}{l_m l_n + l_m l_p + l_n l_p} \right) \times C_{si} \tag{18}$$

Partial derivatives can characterize the rate of change of the cost function in the X direction, improving the efficiency of selecting the segmentation plane during spatial segmentation.

IV. B. 2) Three-dimensional visualization scene modeling

Based on the aforementioned spatial partitioning algorithm, three-dimensional visualization scene modeling for the three-dimensional control platform can be completed. In actual scheduling and operation and maintenance, the tooling of effective operation and maintenance management methods has become one of the urgent issues that the three-dimensional control platform needs to solve. Through the implementation of software and hardware systems, functional modules such as asset lifecycle management, resource capacity management, and energy consumption management can be realized to manage the data center and optimize its performance, while fully utilizing data to improve operation and maintenance efficiency and reliability. The core features of this technology are: establishing a 3D visualization operations and maintenance scene and giving it interactivity and interactivity, specifically including the following steps:

(1) Enclose the 3D visualization operations and maintenance scene with an AABB-type scene bounding box

(2) Establish a cost function

(3) Divide the scene through the cost function

(4) Reconstructing the three-dimensional scene model with Unity3D interface communication.

(5) Implementing operations and maintenance tasks through interface communication. Through the above steps, scene organization can be achieved. From the three-dimensional control platform visualization interaction technology described in this paper, a binary tree structure is used for scene association and organizational management. Using this structure, existing mature tree preorder, inorder, or postorder traversal algorithms can be applied to access all scenes.

IV. B. 3) Visualization Management Implementation

When implementing the visualization system interface, the MVC architecture was used in the software architecture. This framework has the advantages of low coupling, high reusability, strong maintainability, and is conducive to software engineering management. In addition, the system also uses Unity 3D technology, a professional 3D scene rendering engine developed by Unity Technologies. The 3D control platform uses this technology and scene segmentation algorithms to write programs in JavaScript and assign them as components to virtual objects.

IV. C. Visualization Control Technology Testing

IV. C. 1) Grid operation data rewriting and reading test

(1) Data Rewrite Test

During power grid operations, a large amount of real-time data is generated, placing high demands on data storage and access. When inserting data, if the time required per unit of data is $T1$ and the time required for 10,000 data points is $T2$, the following inequality must be satisfied for effective utilization of the 3D control platform in 3D visualization system data management: $T2 < T1 \times 1000$. Taking UPS data testing as an example, the relationship between data capacity and response time was tested, with results shown in Figure 9. Different colored surfaces correspond to different data volumes. Under the condition of the same data volume per modification, the larger the total data capacity, the longer the processing time. The maximum response times for data capacities of 5 million, 7 million, and 10 million records are 25 μs, 35 μs, and 50 μs, respectively. If the data volume modified in a single operation exceeds 1 million records, the processing time is approximately 12 μs. When the data volume modified in a single operation exceeds 2 million records, the processing time can be reduced to 7.87 μs, and the processing time tends to stabilize, with minimal differences in processing time across different total data volumes.

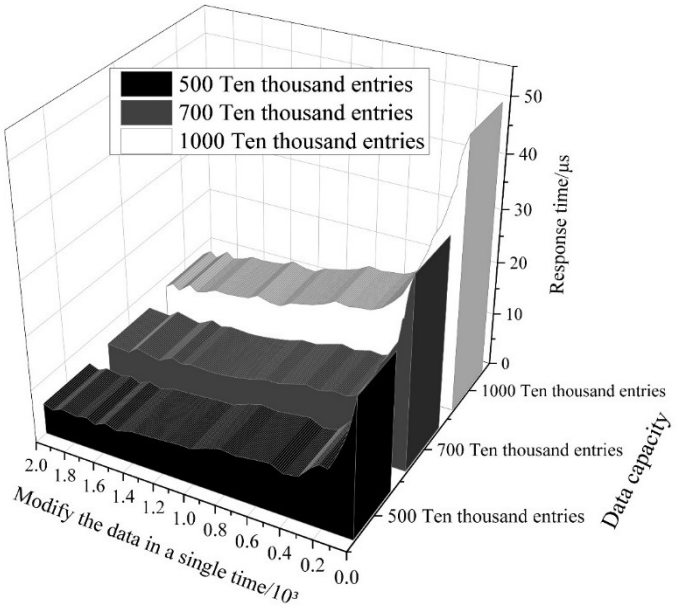

Figure 9: Data rewriting test

(2) Information Reading Test

Figure 10 shows the grid information reading test, which illustrates the relationship between data volume and response time in data reading tests. As the query data volume increases, the response time continues to increase. When the data volume reaches 100,000 records, the response time reaches 25 ms; when the data volume reaches 200,000 records, the response time reaches 60 ms; and when the data volume reaches 400,000 records, the response time approaches 120 ms. It can be seen that the two exhibit an approximate linear relationship, but not a strict linear relationship, with some fluctuation characteristics. This phenomenon may be influenced by factors such as the complexity of the power grid data structure and index efficiency.

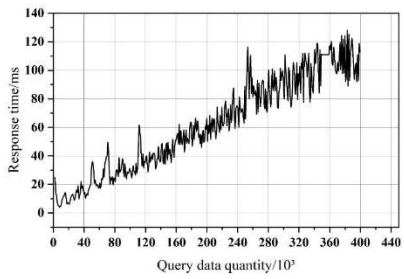

Figure 10: Grid information reading test

In summary, in terms of data management for the three-dimensional visualization system of power grid information, the three-dimensional control platform designed in this paper, as an information storage medium, has appropriate scalability in terms of data insertion, data reading, and data rewriting, and can be used for real-time processing of system data.

IV. C. 2) Switching Time Test

To validate the feasibility of a visualization and control method for power information systems based on 3D modeling, we introduced spatial segmentation visualization and control methods and intelligent dispatch visualization and control methods for comparison, and tested the capabilities of the power information system in terms of visualization switching time and visualization and control accuracy.

Since the power information system involves regional power safety, a simulation system was constructed based on a power information system prototype and tested on the EMTDC simulation platform. This platform is fully functional, highly compatible, and can run on Windows systems.

To verify the performance of the methods proposed in this project in power information system visualization, visualization switching time was used as the experimental indicator. Based on the aforementioned experimental environment, the switching performance of the three methods was tested, with the results shown in Figure 11.

As the response time of the power information system changes, the visualization switching time of the power information system visualization control method based on three-dimensional modeling is the shortest, below 1.4 seconds. In contrast, due to the inability of the spatial segmentation visualization control method to estimate the operational status of the power information system, the error between the sampled power data values and the actual values increases, leading to delays in the visualization switching of the power information system, with the maximum switching time reaching 4.04 seconds. The intelligent dispatch visualization control method does not perform visualization processing on the power information system. As the system response time changes, visualization switching commands cannot be immediately transmitted to the visualization switching interface, thereby extending the visualization switching time of the power information system, with the maximum switching time approaching 3 seconds.

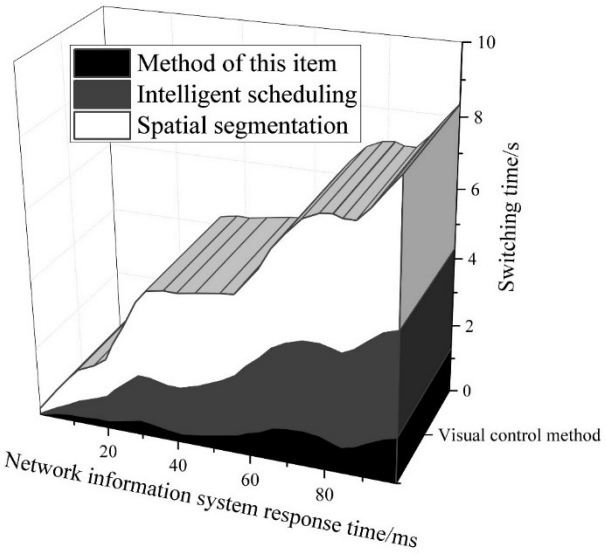

Figure 11: The test results of the visual switching time of the power information system

IV. C. 3) Visualization Management Accuracy Test

In the simulation platform, the corresponding power information management and control is carried out using the methods of this project. The accuracy of the management and control is evaluated through simulation software. The test results for the visualization management and control accuracy of the power information system are shown in Figure 12.

In terms of visualization control accuracy for the power information system, the test results for the spatial segmentation visualization control method and the intelligent scheduling visualization control method are very similar. However, since the spatial segmentation visualization control method completely disregards the requirements of the power information system during application, it results in disorganized power data within the system, thereby reducing the visualization control accuracy of the power information system. In contrast, the power information system visualization control method proposed in this paper (3D modeling) comprehensively considers

the requirements of the power information system and the spatial segmentation of the scene, enabling power data to be segmented according to specific categories or properties. This enhances the orderliness of power data, gradually improving the visualization control accuracy of the power information system. When the response time of the power information system is 90ms, the control accuracy reaches 96.85%.

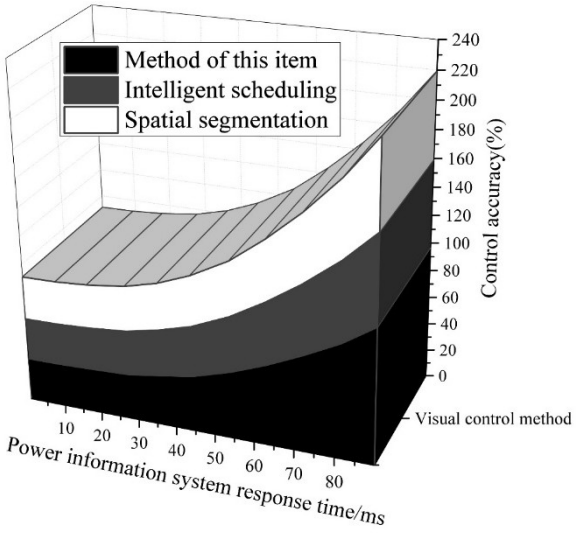

Figure 12: Test results of the visualization control accuracy of the power information system

V. Conclusion

This paper establishes and implements a power grid safety management system based on the principles of power grid safety operation management using a three-dimensional control platform. It proposes power grid safety assessment indicators, converts safety levels into quantifiable risk indicators, and calculates safety issues in power grid operation planning. By combining typical system operation modes with component failure models, it derives a safety risk assessment process incorporating system management methods and designs a three-dimensional control platform for power operation safety.

(1) Using the grid safety assessment indicators and the comprehensive linear scoring method, a comprehensive safety score was calculated for grid operation safety. Region 5 had the highest safety level, with a safety score of 0.65485. The N-1 verification pass rate and the positive indicator value for power supply per unit of line length were relatively high, at 94.37486% and 1,338.248 million kW•h/km, respectively. While the expected power shortage value of 7.33487 hours is the minimum value. The evaluation results obtained are consistent with the actual safety of the power grids in each region.

(2) Using simulation experiments to test visualization control technology, the proposed technology in this paper achieves a response time of approximately 7.87 μs when the number of data modifications exceeds 2 million in data modification and information retrieval tests, with the response time tending to stabilize. As the volume of query data increases, the response time continues to grow. When the grid operation data volume reaches 400,000 records, the response time approaches 120 ms, exhibiting an approximately linear relationship between the two.

References

[1] Panteli, M., & Mancarella, P. (2015). The grid: Stronger, bigger, smarter?: Presenting a conceptual framework of power system resilience. IEEE Power and Energy Magazine, 13(3), 58-66.

[2] Dong, K., Yang, R., & An, Z. (2022). Establish a Risk Prevention and Control System for the Maintenance of Communication Optical Cables to Ensure the Safety of Power Grid Operation. International Core Journal of Engineering, 8(8), 988-996.

[3] Zhou, H., Su, Y., Chen, Y., Ma, Q., & Mo, W. (2016). The China southern power grid: solutions to operation risks and planning challenges. IEEE Power and Energy Magazine, 14(4), 72-78.

[4] Hatziargyriou, N., Milanovic, J., Rahmann, C., Ajjarapu, V., Canizares, C., Erlich, I., ... & Vournas, C. (2020). Definition and classification of power system stability–revisited & extended. IEEE Transactions on Power Systems, 36(4), 3271-3281.

[5] Fang, J., Li, H., Tang, Y., & Blaabjerg, F. (2018). On the inertia of future more-electronics power systems. IEEE Journal of Emerging and Selected Topics in Power Electronics, 7(4), 2130-2146.

[6] Yu, X., & Xue, Y. (2016). Smart grids: A cyber–physical systems perspective. Proceedings of the IEEE, 104(5), 1058-1070.

[7] Albarrak, A. M. (2024). Integration of Cybersecurity, Usability, and Human-Computer Interaction for Securing Energy Management Systems. Sustainability (2071-1050), 16(18).

[8] Fan, S., Guo, J., Ma, S., Li, L., Wang, G., Xu, H., ... & Zhao, Z. (2023). Framework and Key Technologies of Human-machine Hybrid-augmented Intelligence System for Large-scale Power Grid Dispatching and Control. CSEE Journal of Power and Energy Systems, 10(1), 1-12.
[9] Adepoju, O., Akinyomi, O., & Esan, O. (2023). Integrating human-computer interactions in Nigerian energy system: A skills requirement analysis. Journal of Digital Food, Energy & Water Systems, 4(2).
[10] Rahman, M. R. (2018). Understanding the human-computer interaction behavior in electrical and power systems. Industrial Safety Management: 21st Century Perspectives of Asia, 143-151.
[11] Gołębiewski, D., Barszcz, T., Skrodzka, W., Wojnicki, I., & Bielecki, A. (2022). A New Approach to Risk Management in the Power Industry Based on Systems Theory. Energies, 15(23), 9003.
[12] Teixeira, A., Sou, K. C., Sandberg, H., & Johansson, K. H. (2015). Secure control systems: A quantitative risk management approach. IEEE Control Systems Magazine, 35(1), 24-45.
[13] Shah, R., Mithulananthan, N., Bansal, R. C., & Ramachandaramurthy, V. K. (2015). A review of key power system stability challenges for large-scale PV integration. Renewable and Sustainable Energy Reviews, 41, 1423-1436.
[14] Panteli, M., Trakas, D. N., Mancarella, P., & Hatziargyriou, N. D. (2017). Power systems resilience assessment: Hardening and smart operational enhancement strategies. Proceedings of the IEEE, 105(7), 1202-1213.
[15] Ning, W., Peng, W., Bingjun, Z., Lin, X., Suo, W., Shuai, Z., ... & Yuan, H. (2020, July). Study on Three-Dimension Design Management of Power Grid Projects Centered on Quality Improvement. In IOP Conference Series: Earth and Environmental Science (Vol. 531, No. 1, p. 012007). IOP Publishing.
[16] Peng, Q. W., Jin, X. L., Xu, C. Q., & Lu, D. (2020, February). The Power Grid Operation Risk Control Application Based on 3D Real-Time Rendering Technology. In 2020 12th International Conference on Measuring Technology and Mechatronics Automation (ICMTMA) (pp. 460-463). IEEE.
[17] Cai, D., He, X., Yu, Z., Wang, L., Xie, G., & Ai, Q. (2015, October). 3D power-map for smart grids—An integration of high-dimensional analysis and visualization. In International Conference on Renewable Power Generation (RPG 2015) (pp. 1-5). IET.
[18] Guo, Y., Yang, Z., Feng, S., & Hu, J. (2018). Complex power system status monitoring and evaluation using big data platform and machine learning algorithms: a review and a case study. Complexity, 2018(1), 8496187.
[19] Jing, F., Li, X., Yuan, Z., Li, B., & Li, Z. (2024, January). 3DE Digital Platform for Electrical Distribution Design of Pumped Storage Power Stations. In 2024 Asia-Pacific Conference on Software Engineering, Social Network Analysis and Intelligent Computing (SSAIC) (pp. 167-171). IEEE.
[20] Duanmu, X., Lan, G., Chen, K., Shi, X., & Zhang, L. (2022, December). 3D Visual Management of Substation Based on Unity3D. In 2022 4th International Academic Exchange Conference on Science and Technology Innovation (IAECST) (pp. 427-431). IEEE.
[21] Bhattarai, B. P., Paudyal, S., Luo, Y., Mohanpurkar, M., Cheung, K., Tonkoski, R., ... & Zhang, X. (2019). Big data analytics in smart grids: state‐of‐the‐art, challenges, opportunities, and future directions. IET Smart Grid, 2(2), 141-154.
[22] Cintuglu, M. H., Mohammed, O. A., Akkaya, K., & Uluagac, A. S. (2016). A survey on smart grid cyber-physical system testbeds. IEEE Communications Surveys & Tutorials, 19(1), 446-464.
[23] Zhou, K., Fu, C., & Yang, S. (2016). Big data driven smart energy management: From big data to big insights. Renewable and sustainable energy reviews, 56, 215-225.
[24] Shen, J., Jiang, C., Liu, Y., Wang, X., & Qian, J. (2016). Microgrid operation optimization with regulation of grid tie‐line power fluctuations and risk management. International Transactions on Electrical Energy Systems, 26(11), 2308-2321.
[25] Lamba, V., Šimková, N., & Rossi, B. (2019). Recommendations for smart grid security risk management. Cyber-Physical Systems, 5(2), 92-118.
[26] Hock, K. P., & McGuiness, D. (2018, June). Future state visualization in power grid. In 2018 IEEE International Conference on Environment and Electrical Engineering and 2018 IEEE Industrial and Commercial Power Systems Europe (EEEIC/I&CPS Europe) (pp. 1-6). IEEE.
[27] Xiao, Y., Fei, Z., Zheng, K., Zhang, T., Qian, B., & Zheng, W. (2019). A Survey of Power Grid Operation State Visualization. Journal of Computer-Aided Design & Computer Graphics, 31(10), 1750-1758.
[28] Zheng, F., Xia, Y., Su, H., & Wang, W. (2021, January). Research on key technologies of power system visualization platform. In 2021 13th International Conference on Measuring Technology and Mechatronics Automation (ICMTMA) (pp. 235-238). IEEE.
[29] Yong, W., Yu, Z., Li, K., & Zhang, F. (2024, December). Research on Visualization Application of Power Data Based on Business Intelligence Technology. In 2024 14th International Conference on Power and Energy Systems (ICPES) (pp. 352-355). IEEE.
[30] Qingwei, M. E. N. G., Hao, S. U. N., Mingxiao, Z. H. U., & Peng, L. I. (2023). Development and experimentation of visualized simulation platform for floating offshore wind power grid-connected system. Experimental Technology and Management, 40(10), 119-127.
[31] Hamed Zeinoddini Meymand,Reza Safipour & Farhad Namdari. (2025). A Novel Management Approach for Optimal Operation of Hybrid AC-DC Microgrid in the Presence of Wind and Load Uncertainties. Systems,13(4),233-233.
[32] Elaheh Yaghoubi,Elnaz Yaghoubi,Mohammad Reza Maghami & Mehdi Zareian Jahromi. (2025). Comprehensive technical risk indices and advanced methodologies for power system risk management. Electric Power Systems Research,244,111534-111534.
[33] Liqiang Wang,Hongqing Liu,Qi Wang,Yu Cong & Xiuxian Zheng. (2024). Evaluation of power system instability probability considering output randomness of grid-connected converter. Journal of Physics: Conference Series,2874(1),012012-012012.
[34] Xingzhen Li,Yiwei Ma,Hao Zhong & Miao Huang. (2025). A Novel Clustering Method for PV Power Curve Patterns based on Multidimensional Feature, Entropy Weight, and K-means. Engineering Letters,33(4),